

Article

Three-Dimensional Thermal Modeling of Internal Shorting Process in a 20Ah Lithium-Ion Polymer Battery

Yubai Li ¹, Zhifu Zhou ² and Wei-Tao Wu ^{3,*}

¹ Department of Mechanical Engineering, Carnegie Mellon University, Pittsburgh, PA 15213, USA; yubail@andrew.cmu.edu

² State Key Laboratory of Multiphase Flow in Power Engineering, Xi'an Jiaotong University, Xi'an 710049, China; zfzhou@mail.xjtu.edu.cn

³ School of Mechanical Engineering, Nanjing University of Science and Technology, Nanjing 210094, China

* Correspondence: weitaowwtw@njust.edu.cn

Received: 20 January 2020; Accepted: 21 February 2020; Published: 24 February 2020



Abstract: To better address the safety issues of a lithium-ion battery, understanding of its internal shorting process is necessary. In this study, three-dimensional (3D) thermal modeling of a 20 Ah lithium-ion polymer battery under an internal shorting process is performed. The electrochemical thermal coupling scheme is considered, and a multi-scale modeling approach is employed. An equivalent circuit model is used for characterizing the subscale electrochemical behaviors. Then, at the cell scale, the electrical potential field and thermal field are resolved. For modeling the internal shorting process, a block of an internal short is directly planted inside the lithium-ion battery. Insights of the temperature evolutions and 3D temperature distributions are drawn from the simulations. The effects of shorting resistance, through-plane thermal conductivity, and mini-channel cold-plate cooling are investigated with the simulations. A large amount of heat generation by a small shorting resistance and highly localized temperature rise are the fundamental thermal features associated with the internal shorting process. The through-plane thermal conductivity plays an important role in the maximum temperature evolutions inside the battery cell, while the external cooling condition has a relatively weak effect. But the cold plate cooling can benefit lithium-ion battery safety by limiting the high temperature area in the internal shorting process through heat spreading.

Keywords: lithium-ion battery; thermal abuse; internal shorting; thermal modeling; safety; mini-channel cooling

1. Introduction

Lithium-ion battery powered electric vehicles (EVs) and hybrid electric vehicles (HEVs) pose a promising choice in the worldwide trend of transportation electrification. The electrified mobility can significantly reduce the petroleum reliability and carbon intensity in transportation. A lithium-ion battery works within a narrow domain of temperature. Under temperature below zero degrees Celsius, like $-30\text{ }^{\circ}\text{C}$, the performance of a lithium-ion battery will be severely lowered [1]. On the other hand, under high temperature, like $50\text{ }^{\circ}\text{C}$, the lithium-ion battery will suffer capacity and power fade, and under even more elevated temperatures like $100\text{ }^{\circ}\text{C}$, the lithium-ion battery will suffer thermal runaway [2]. Thus, for better adoption of lithium-ion batteries in EVs and HEVs, better understanding the thermal effects of the lithium-ion battery and providing appropriate thermal management of the battery are essential [2]. Mathematical modeling and numerical simulations are important for predicting and understanding the thermal behaviors of lithium-ion batteries and for providing the appropriate thermal management solutions [3]. Karimi and Li [4] studied various

cooling strategies towards thermal management of a lithium-ion battery for electric vehicles. The heat generation from a lithium-ion battery was accounted for with approximations of battery internal resistances and entropy changes, and the heat transfer characteristics of the natural convection cooling, the forced convection cooling, and the phase change material (PCM) on a lithium-ion battery pack were elucidated. For better capturing the electrochemical thermal interactions in a lithium-ion battery, more sophisticated physics-based thermal models for a lithium-ion battery have also been proposed. Many electrochemical thermal coupled lithium-ion battery models are based on the famous Newman 1 + 1D lithium ion model [5,6], and such models have been extended to multi-dimensional lithium-ion battery model with the modeling platforms of COMSOL Multiphysics [7,8], ANSYS Fluent [9,10], and other platforms [11,12]. The electrochemical thermal coupled lithium-ion battery model offers a powerful tool and has been widely applied for studying lithium-ion battery and lithium-ion battery pack thermal management [13–18].

Today, safety is one of the most critical challenges for wider lithium-ion battery application in EVs and HEVs. Thermal runaway is the major issue in lithium-ion battery safety. The thermal runaway in a lithium-ion battery is triggered by elevated temperature. Under the elevated temperature, an exothermic reaction will occur and generate heat. When the heat exceeds the thermal diffusion, a further increase of temperature will occur and more exothermic reactions will be triggered [19]. Various abusive conditions, such as mechanical abuse, electrical abuse and thermal abuse can cause thermal runaway of a lithium-ion battery [20]. In a lithium-ion battery pack, especially a high-energy battery pack with large-format lithium-ion batteries, the thermal runaway can propagate between batteries [21,22] and lead to a catastrophic fire or explosion [23]. Thus, understanding the thermal behaviors respect to the lithium-ion battery thermal runaway is vital for preventing the thermal runaway or reduce the hazardous impacts from thermal runaway [24]. Experimental testing such as overcharging, heating test, and nail penetration are typical approaches for investigating lithium-ion battery responses under those conditions [19].

Except for the experimental testing, thermal modeling provides another approach to study the mechanisms of the lithium-ion battery under abusive conditions and to find the solutions to suppress the thermal runaway. The modeling methods of a lithium-ion battery can be basically summarized into two categories. In one category, the reaction kinetics of the exothermic reactions are emphasized and the electrochemical model is not coupled into a thermal abuse model. Hatchard et al. [25] developed an early 1D thermal abuse model based on reaction kinetics and electrode heat generation rate. The model predicted the lithium-ion battery cell thermal responses under oven exposure testing well compared with experimental data. Spotnitz and Franklin [26] provided a comprehensive survey of abuse testing of lithium-ion cells and components and gave complete estimations of heat of reactions for a set of exothermic reactions. Then the thermal responses of a lithium-ion battery under abusive conditions of an oven, short-circuit, overcharge, nail, and crushing were investigated with a 1D thermal abuse model they built. Kim et al. [27] extended thermal abuse model to 3D finite volume method (FVM)-based lithium-ion battery model that can capture the impacts of non-uniform distributions, thermal and electrical path design, localized heating and cooling, as well as battery materials and geometric configurations. They simulated and investigated the exothermic reactions spreading inside a lithium-ion battery considering a localized heat release. Guo et al. [28] established a 3D lithium-ion battery thermal abuse model based on the finite element method (FEM). An oven test condition was subjected under simulation and it demonstrated the LiFePO_4 cathode is thermally more stable than the LiCoO_2 cathode, and the shutdown mechanisms of separators can alleviate thermal runaway. Recently, the 3D thermal abuse models have also been built in studies [29–33] to investigate the effects of cell physical configuration and electrolyte combustion [29], mini-channel cooling [30], mechanical abuse and cell deformation [31] under a thermal runaway, and the thermal runaway propagation between lithium-ion battery cells [32,33].

In another category of lithium-ion battery thermal abuse models, the electrochemical model and the electrochemical thermal coupling are considered to study the internal shorting or nail-penetration

processes. An internal short circuit can be caused by various manufacturing defects such as conductive particle wound in the jelly roll or wrinkle in the separator [19]. Even without manufacturing defects, the internal short is also one of the most common features under all the lithium-ion battery abuse conditions [20]. The internal short is highly dangerous for triggering lithium-ion battery thermal runaway, and no electronic device can protect the cell against internal shorting conditions [19]. The nail penetration test is a test designed to simulate and to investigate an internal short in a lithium-ion battery [19]. The internal shorting process is at the initiation period of thermal runaway, is highly transient, and enrolls electrochemical thermal effect coupling by its nature. Thus, modeling of the internal shorting process or the nail-penetration process is urgently needed to understand this very important period of internal short in lithium-ion battery without the extensive cost of experimental implementation. Santhanagopalan et al. [34] developed a 2D electrochemical thermal model to study the internal shorting process. It was found that the short between the lithiated anode material and the aluminum current collector would result in maximum heat generation. In addition, the larger capacity of cell and higher state of charge would generate more heat due to the greater potential difference between electrodes. Zavalis et al. [35] built up a 2D coupled electrochemical-thermal model to study the effect of the external shorting, nail penetration and impurity-induced short circuit scenarios. One layer of the anode-separator-cathode sandwich structure was modeled and it was observed that the current determines the rate of the temperature rise. Zhao et al. [36,37] recently established a 3D electrochemical-thermal coupled model to study the nail-penetration process [36] and the internal shorting process [37] in large-format lithium-ion batteries. Clear 3D thermal contour evolutions on large-format lithium-ion batteries were predicted and several critical effects in the nail-penetration process and internal shorting process were revealed in their study. In summary, the development of 3D electrochemical thermal model for the lithium-ion battery internal shorting process is still at early stage and more studies are needed.

In this study, 3D thermal modeling of the internal shorting process in a 20 Ah large format lithium-ion polymer battery is conducted. The internal short circuit is directly planted inside the large format lithium-ion battery as a separate block in the geometry and mesh. This inside planting method for modeling the internal shorting process has not been used in previous literatures. The direct blocking, meshing, and simulations of the internal short create a condition that mimics the realistic internal shorting process. A multi-scale multi-domain lithium-ion battery model [38] is employed. At the anode-separator-cathode sandwich layers subscale, an equivalent circuit model (ECM) [39] is used to model the electrochemical behaviors. At the regular scale, the electrical fields and thermal fields are solved for the large format lithium-ion battery. The interactions between the subscale and the cell scale are through the volumetric current-transfer rate, the electrochemical heat-generation rate, and the electrical heat-generation rate [38]. Then, the effects of the internal shorting resistance, the through-plane thermal conductivity of the large format lithium-ion battery, and the mini-channel cold-plate cooling are carefully discussed with the simulations. For the case with mini-channel cold-plate cooling, conjugate heat transfer has been considered.

2. Modeling Method

The difficulty of lithium-ion battery modeling comes from its enrollment of multi-scale and multi-physics. A multi-scale multi-domain lithium-ion battery modeling framework is adopted for the present study. For the subscale model, the ECM approach is used. In the ECM approach, the behavior of a lithium-ion battery is represented by an electrical circuit, as shown in Figure 1a. The ECM approach has been demonstrated to be an effective method to model the subscale electrochemical characteristics of lithium-ion batteries with accuracy and robustness [40]. The schematics of geometry and mesh for the lithium-ion battery thermal modeling are shown in Figure 1b,c. Except for the scales shown in Figure 1, the thickness of the battery cell is 7.2 mm while the thickness of the tab area is assumed to be 4.32 mm. The geometry is set up based on an EiG ePLB C020 lithium-ion polymer battery. The ePLB C020 is a high energy-density lithium-ion battery based on $\text{Li}[\text{NiCoMn}]\text{O}_2$ cathode

and graphite anodes. It has a format of prismatic, nominal voltage of 3.65 V, and nominal capacity of 20 Ah. More specifications of ePLB C020 lithium-ion polymer battery can be found in ref [41]. The mathematical formulation of the ECM approach is:

$$V(t) = V_{OCV} - V_{tran,s} - V_{tran,l} - R_{series}I(t) \quad (1)$$

$$\frac{dV_{tran,s}}{dt} = -\frac{1}{R_{tran,s}C_{tran,s}}V_{tran,s} - \frac{1}{C_{tran,s}}I(t) \quad (2)$$

$$\frac{dV_{tran,l}}{dt} = -\frac{1}{R_{tran,l}C_{tran,l}}V_{tran,l} - \frac{1}{C_{tran,l}}I(t) \quad (3)$$

$$\frac{d(SOC)}{dt} = \frac{I(t)}{3600Q_{ref}} \quad (4)$$

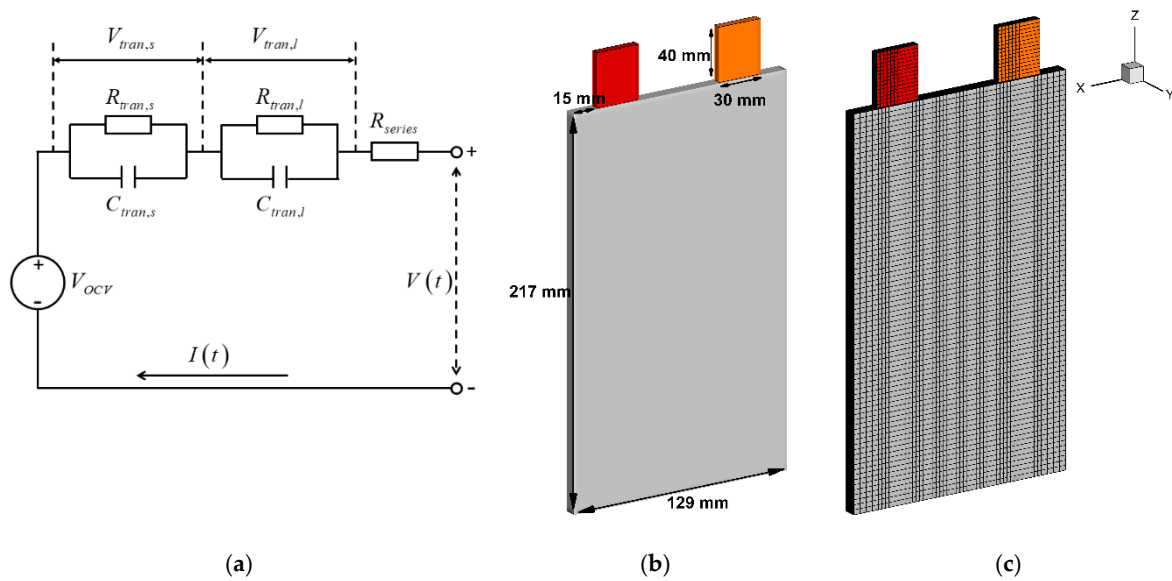


Figure 1. Schematic of (a) equivalent electrical circuit; (b) geometry; (c) mesh of multi-scale multi-domain lithium-ion battery thermal modeling.

In these equations, $V(t)$, $I(t)$, and V_{OCV} are the output voltage, the current, and the open circuit voltage. As illustrated in Figure 1a, the electrical circuit consists of a series resistor R_{series} and two RC parallel network composed of $R_{tran,s}$, $C_{tran,s}$, $R_{tran,l}$, and $C_{tran,l}$, with voltage of $V_{tran,s}$ and $V_{tran,l}$. And the V_{OCV} , R_{series} , $R_{tran,s}$, $C_{tran,s}$, $R_{tran,l}$, $C_{tran,l}$ are formed as functions of state of charge (SOC). The experimental data of the I-V performance and thermal responses for the ePLB C020 cell [42] with different discharging rate is used to fit the parameters. The functions of SOC and the fitted parameters can be found in the equations:

$$V_{OCV} = 3.5 + 0.31SOC - 0.0178SOC^2 + 0.3201SOC^3 - 1.031exp(-24 SOC) \quad (5)$$

$$R_{series} = 0.035 + 0.1562exp(-24.37 SOC) \quad (6)$$

$$R_{tran,s} = 0.04669 + 0.3208exp(-29.14 SOC) \quad (7)$$

$$C_{tran,s} = 703.6 - 752.9exp(13.51 SOC) \quad (8)$$

$$R_{tran,l} = 0.04984 + 6.604exp(155.2 SOC) \quad (9)$$

$$C_{tran,l} = 4475 - 6056exp(27.12 SOC) \quad (10)$$

With these parameters, the modeling results match well with the experimental results [42] of the I-V curve and thermal responses in Figure 2a. In addition, the time variation in the current is tested by another simulation with a pulse waveform of current discharging condition used in reference [43]. In reference [43], the ePLB C020 cell was tested by a protocol that subjects the cell under 15 A pulse discharging for 5 min, and then rests the cell by 15 min before the next discharging period. Then, the simulation results are compared with the experimental results of the cell voltage in Figure 2b to further demonstrate the validity of the present model. The time step for the simulation has been found to be fine enough to capture the battery behavior under such a test protocol. It can be seen in Figure 2b that the modeling results have some differences to the experimental results. As the modeling parameters are fitted from experimental data [42], the predicted voltage does not match perfectly with the experimental results in Figure 2b. If the two experimental datasets are directly compared, they show some slight differences. The differences may come from different experimental conditions and experimental measurement instrumentation. Although all the data are collected from an EiG ePLB C020 lithium-ion polymer battery, the differences between different experiments may come from different contact resistances, different state of aging for tested battery, or from the batch-to-batch battery difference. However, the Figure 2b indicates that the present model captures well the trend of voltage response under pulse wave load condition indeed, which is meaningful. It is also worthwhile mentioning that the predicted average temperature in the battery cell is not compared with experimental data in Figure 2b as the temperature responses are not measured in reference [43]. The predicted temperature is intended to show the battery thermal model behavior under dynamic load condition instead of further validating the battery thermal model. At the lithium-ion battery-cell scale, the electrical equations and thermal equation are solved for the electrical and thermal fields:

$$\nabla \cdot (\sigma_+ \nabla \Phi_+) = -j \quad (11)$$

$$\nabla \cdot (\sigma_- \nabla \Phi_-) = j \quad (12)$$

$$\rho c_p \frac{\partial T}{\partial t} = \frac{\partial}{\partial x} \left(k_{\text{in-plane}} \frac{\partial T}{\partial x} \right) + \frac{\partial}{\partial y} \left(k_{\text{through-plane}} \frac{\partial T}{\partial y} \right) + \frac{\partial}{\partial z} \left(k_{\text{in-plane}} \frac{\partial T}{\partial z} \right) + \dot{q} \quad (13)$$

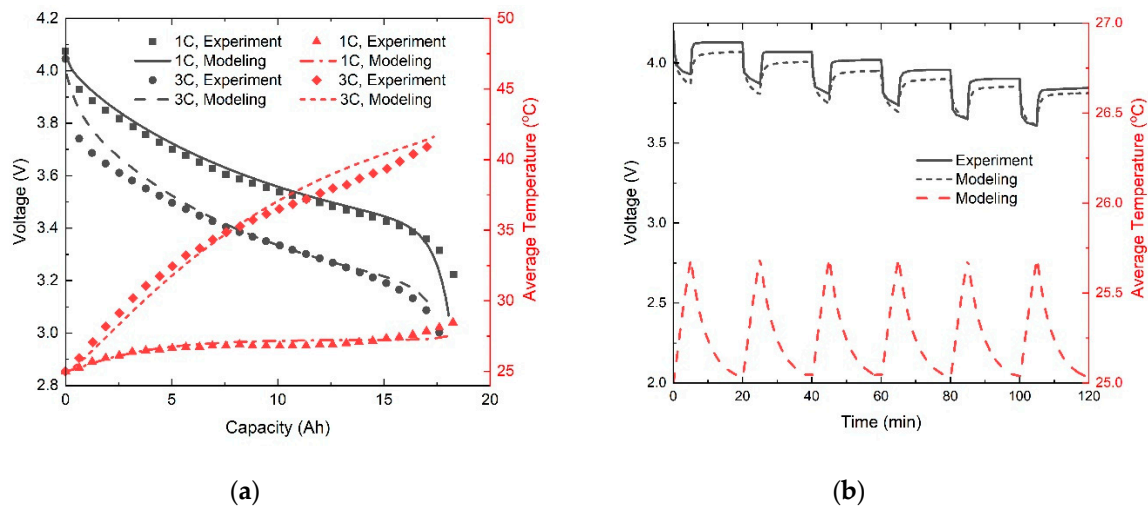


Figure 2. Model validation with experimental data. (a) Constant current discharging; (b) pulse waveform current discharging.

In these equations, σ_+ , σ_- , Φ_+ , Φ_- are the effective electrical conductivities and phase potential for the positive and negative electrode, while j and \dot{q} are the volumetric transfer current density and heat source terms. In the thermal equation, the thermal conductivity is assumed to be non-isotropic [41]. For the large format lithium-ion polymer battery of ePLB C020, it has an internal configuration of

multi-layered structures where the negative and positive electrodes are alternatively wrapped by the continuous separator [41]. Thus, its in-plane thermal conductivity $k_{\text{in-plane}}$ and through-plane conductivity $k_{\text{through-plane}}$ are highly different. The through-plane thermal conductivity is typically much smaller than the in-plane thermal conductivity as the through-plane direction goes across the multi-layer (including low thermal conductivity separator layer) structure. The subscale and the battery cell scale are then connected by the volumetric current transfer rate and the heat source terms, expressed by the following equations:

$$j = I \frac{Q_{\text{total}}}{Q_{\text{ref}} VOL} \quad (14)$$

$$\dot{q} = j \left[V_{\text{OCV}} - (\Phi_+ - \Phi_-) - T \frac{dU}{dT} \right] + \sigma_+ \nabla \Phi_+ \cdot \nabla \Phi_+ + \sigma_- \nabla \Phi_- \cdot \nabla \Phi_- \quad (15)$$

where Q_{total} is the total capacity, Q_{ref} is the reference capacity, VOL is the cell volume, and U is the equilibrium potential. For all the simulations in this work, except the mini-channel cooling condition, the convective cooling for the lithium-ion battery cell is considered. Thus, the convective boundary condition at the battery cell wall is applied with the expression:

$$k_n \frac{\partial T_w}{\partial n} = h_f (T_w - T_f) \quad (16)$$

where T_w is the cell wall temperature, n is the normal direction towards the wall, k_n is the thermal conductivity in the normal direction, T_f is the ambient fluid temperature, and h_f is the heat transfer coefficient. In this study, the T_f is assumed to be 25 °C, while the specific value of h_f is specified in the discussion section. The key electrical and thermal properties assumed in this study are listed in Table 1. In Table 1, the values of the cell density ρ , the cell heat capacity c , the in-plane thermal conductivity $k_{\text{in-plane}}$, and the through plane thermal conductivity $k_{\text{through-plane}}$ are from reference [41]. The values of σ_+ and σ_- are from reference [44].

Table 1. Physical properties for the lithium-ion battery cell.

ρ (kg/m ³)	c (J/kg/K)	$k_{\text{in-plane}}$ (W/m/K)	$k_{\text{through-plane}}$ (W/m/K)	σ_+ (S/m)	σ_- (S/m)
2126	1301	26.57	0.97 (if not specified)	1.19×10^6	9.83×10^5

For the modeling of the internal shorting process, an actual internal short block is planted into the battery geometry. The geometry and mesh considering the internal short are shown in Figure 3. The scale and dimensions of the internal short are shown in Figure 3, and except for the scale indicated, the thickness of the internal short is assumed to be 1.44 mm. By electrically connecting the internal short by an assigned resistance, the internal shorting process can be mimicked. The distributions of the Φ_+ and Φ_- in the lithium-ion battery cell under normal discharging and internal shorting conditions are shown in Figure 4. The current transfer inside lithium-ion battery is driven by the potential gradient. As indicated in Figure 4, the current flow comes from the tab, goes into the whole cell, and goes back to the tab under normal discharging condition. On the other hand, under an internal shorting situation, the current concentrates towards the internal short. The shorting resistance is supposed to be small. Thus, a very large current goes through the internal short in the internal shorting process. The large current will then cause a sudden generation of heat, as seen in the following equation:

$$q_{is} = I_{is}^2 R_{is} / V_{is} \quad (17)$$

where V_{is} , R_{is} , I_{is} , and q_{is} are the values of voltage on the shorting resistance, the shorting resistance quantity, the current passing the shorting resistance, and the electrical heat generated by the shorting resistance.

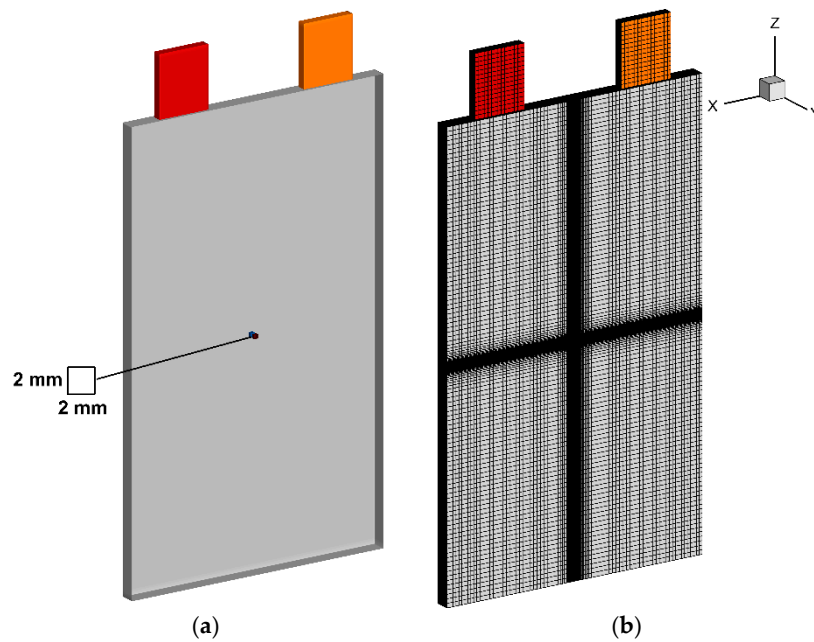


Figure 3. Schematic of (a) geometry; (b) mesh of internal shorting process modeling.

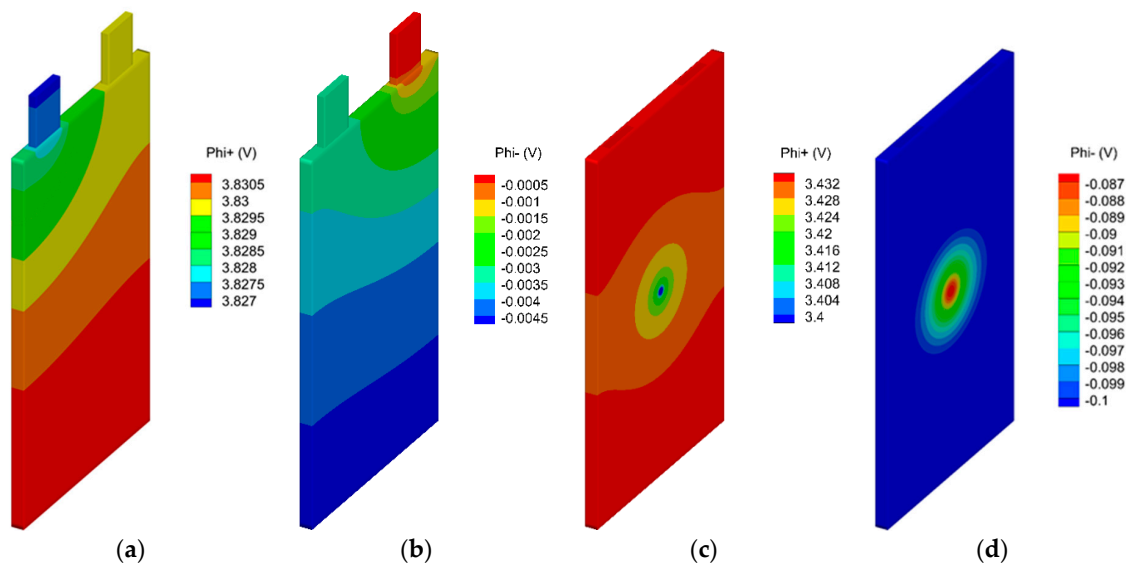


Figure 4. Distributions of (a) Φ_+ under 1C discharging; (b) Φ_- under 1C discharging; (c) Φ_+ under internal shorting by 0.01 Ω ; (d) Φ_- under internal shorting by 0.01 Ω .

The 3D thermal simulations in this study are performed with ANSYS Fluent, while the mesh for the simulations are created with ANSYS ICEM. For the lithium-ion battery with internal short and convective cooling condition, a mesh of 387 k is used for all the simulations, and for the lithium-ion battery with mini-channel cold plate cooling, a mesh of 1.79 million is used. A time step of 0.1 s is used for simulating the initial 60 s behaviors of the internal shorting process. For studying the effects of shorting resistances on the internal shorting process, simulations are made by keeping all the other conditions to be identical, while assigning internal short resistances of 0.005 Ω , 0.01 Ω , 0.015 Ω , 0.02 Ω , and 0.03 Ω . For studying the effects of through-plane thermal conductivity on the internal shorting process, a series of simulations of the internal shorting processes with shorting resistances of 0.01 Ω are conducted. All the other conditions are kept identical, and the through-plane thermal conductivity of 0.97 W/m/K [41], 2.0 W/m/K, 5.0 W/m/K, and 10.0 W/m/K are subjected under simulations. For investigating the effects of mini-channel modeling, a series of simulations

are made under shorting resistance of 0.01Ω . The reference condition is with the convective heat transfer coefficient of $17 \text{ W}/(\text{m}^2 \cdot \text{K})$. Another case with convective boundary condition and heat transfer coefficient of $30 \text{ W}/(\text{m}^2 \cdot \text{K})$ is also performed. These two cases represent the typical air-cooling condition and are used for comparison. Another two cases with mini-channel cold plate are simulated, and the inlet coolant velocity are assumed to be 0.05 m/s and 0.1 m/s .

3. Results and Discussions

3.1. Effect of Shorting Resistance

The thermal responses of a lithium-ion battery in the internal shorting process is affected largely by the shorting resistance, as implied by the analysis implied in Equation (17). Different shorting resistances in the range of 0.005Ω to 0.03Ω are subjected to simulations to provide a trend analysis of the shorting resistance effects on the internal shorting process. Such a study aims to help point out that internal shorting can be extremely harmful for a small shorting resistance, while the internal shorting is not that harmful with a resistance larger than a certain value. A basis of the assumption comes from reference [37], which estimates the internal shorting resistance to be about 0.005Ω ($5.3 \text{ m} \Omega$). This supports the assumption of shorting resistance range chosen in this study. The modeling predicted temperature evolutions are shown in Figure 5a. It is seen that internal short resistance has a dominating effect for the temperature response. Shorting resistances of 0.005Ω and 0.01Ω can cause the maximum cell temperature to reach $800 \text{ }^\circ\text{C}$ and $300 \text{ }^\circ\text{C}$ within 10 s. Such a high temperature will trigger aggressive further thermal runaway. As the temperature above $100 \text{ }^\circ\text{C}$ can already initiate thermal runaway, the shorting resistance of 0.015Ω and 0.02Ω can also cause further thermal runaway as indicated in this study. On the other hand, for the internal short resistance of 0.03Ω , the temperature responses for the lithium-ion battery cell is more like the normal discharging condition which will not trigger thermal runaway. It is found that the thermal behaviors of a lithium-ion battery cell are very sensitive to the quantity of shorting resistance. In addition, the shorting resistance may actually vary with time due to the temperature variation. It is hard indeed to estimate how the shorting resistance changes with time. For a preliminary study on the resistance variation's effect on internal shorting, two more cases are performed assuming linear changing of the shorting resistance from 0.01Ω to 0.005Ω , or 0.02Ω within a period of 60 s. The temperature response is shown in Figure 5b. Those simulations give the demonstration for the incorporation of the resistance variation. However, further effort is still needed to establish the internal shorting resistance correlation with temperature.

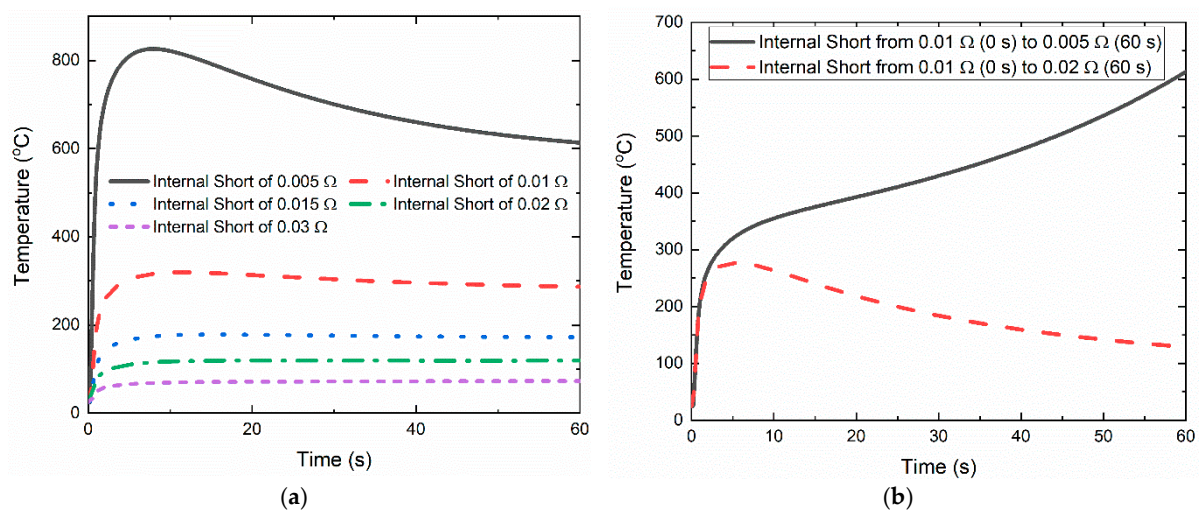


Figure 5. Modeling predicted maximum temperature evolutions on the lithium-ion battery cell under (a) different internal shorting resistances; (b) internal shorting resistance variation.

The temperature contour evolutions on the lithium-ion battery cell surface under internal shorting by 0.01Ω and 0.02Ω are shown in Figures 6 and 7. The temperature near the internal short increases suddenly within 10 s, and then the temperature spreads to the larger area inside the cell by heat conduction. It is found that the temperature responses for a lithium-ion battery cell under a internal shorting condition is a localized behavior. Under both 0.01Ω and 0.02Ω shorting resistances, for the period of 60 s, most of the lithium-ion battery cell remains at moderate temperature. The dangerous temperature is seen within a certain area surrounding the internal short. The thermal features of the internal shorting process are quite special compared with the typical problems faced in lithium-ion battery thermal management. For typical lithium-ion battery cooling, a relatively uniform heat release is expected. Thus, relatively uniform cooling solutions are usually provided like air cooling or a single phase cold plate. The results in this study reveal the thermal behaviors of an internal shorting process, which releases a large amount of heat in a short time period and induces localized high temperature.

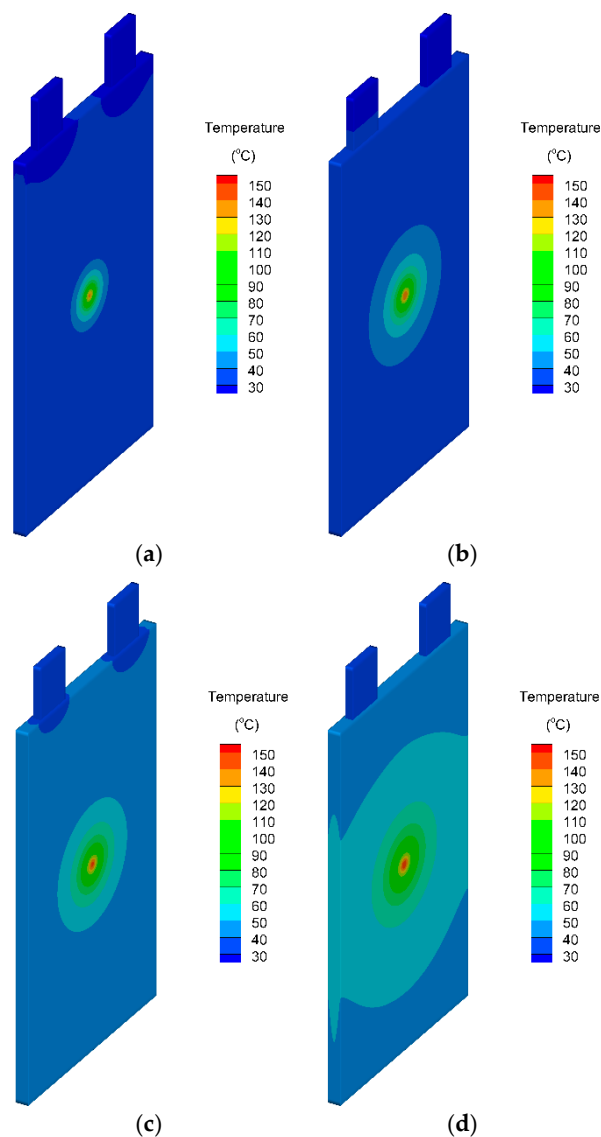


Figure 6. Temperature distributions of lithium-ion battery under internal shorting by 0.01Ω after periods of (a) 15 s; (b) 30 s; (c) 45 s; (d) 60 s.

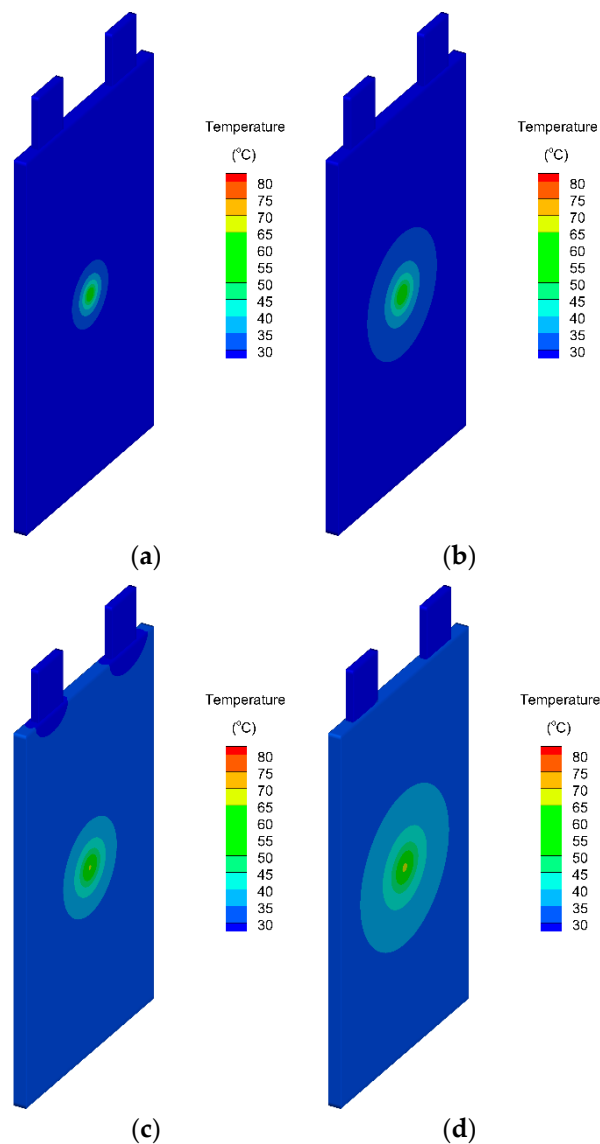


Figure 7. Temperature distributions of lithium-ion battery under internal shorting by 0.02Ω after periods of (a) 15 s; (b) 30 s; (c) 45 s; (d) 60 s.

3.2. Effect of Through-Plane Thermal Conductivity

The thermal conductivity of a lithium-ion battery has important impacts on the temperature evolution and the temperature distributions in the battery cell. As mentioned, the through-plane thermal conductivity in lithium-ion battery is much smaller than the in-plane thermal conductivity, which poses a large resistance for the heat to be conducted out to the cell surface. Thus, the effects of through-plane thermal conductivity on the lithium-ion battery thermal responses under the internal shorting process are specifically discussed with modeling. Figure 8 shows the evolution of the maximum temperature on the lithium-ion battery cell. It is seen that the through-plane thermal conductivity greatly affects the temperature response in the internal shorting process. For the case with through-plane thermal conductivity of 0.97 W/m/K , the maximum temperature in the cell exceeds $300 \text{ }^\circ\text{C}$, while for the case with 10.0 W/m/K thermal conductivity, the maximum temperature in the cell is about $200 \text{ }^\circ\text{C}$. It is found that enhancing the through-plane thermal conductivity can effectively reduce the battery temperature in an internal shorting process.

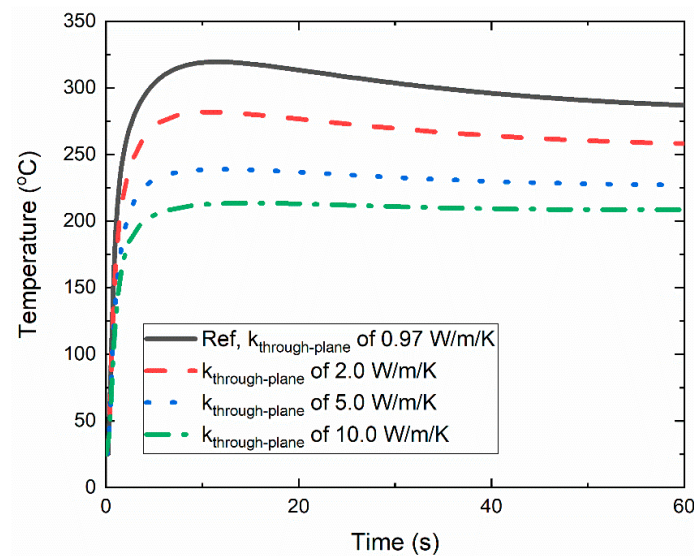


Figure 8. Modeling predicted maximum temperature on lithium-ion battery cell with different through-plane thermal conductivities.

The reason for such large impacts can be explained with Figure 9, which shows the through-plane temperature distributions from the internal short and cell interface to the lithium-ion battery cell wall. It is seen that the low through-plane thermal conductivity of 0.97 W/m/K results in a steeper through-plane temperature distribution. The temperature distribution is caused by large conduction heat resistance in the through-plane direction; while for the through-plane thermal conductivity of 10.0 W/m/K, this resistance is significantly lowered, as observed in Figure 9. The modeling work implies that even with a very high convective heat transfer coefficient achieved on the lithium-ion battery cell surface, the internal temperature of a lithium-ion battery cell can still be high. The large amount of heat generated from the internal short cannot be easily conducted out to the surface. The temperature rise inside the lithium-ion battery cell near the internal short will still trigger thermal runaway. This means that except for the external cooling design, the internal mechanisms and internal suppression of the temperature rise have significant importance in mitigation of the internal shorting induced thermal runaway.

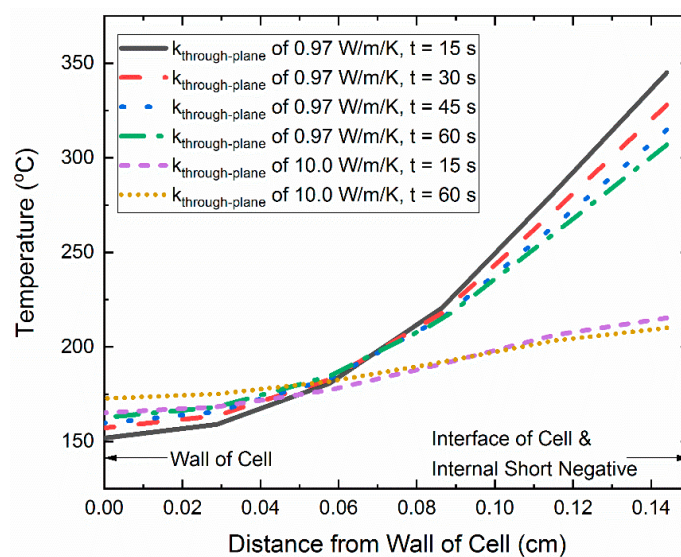


Figure 9. Modeling predicted temperature distributions in through-plane direction with through-plane thermal conductivities of 0.97 W/m/K and 10.0 W/m/K.

3.3. Effect of Mini-Channel Cold-Plate Cooling

In the previous simulations, the convective heat-transfer boundary condition is considered at the battery cell wall. The convective heat-transfer boundary condition reflects more on the air cooling condition for the lithium-ion battery. Another major cooling method for lithium-ion battery and lithium-ion battery pack is the mini-channel cold plate. To investigate the effect of mini-channel cold-plate cooling on the lithium-ion battery thermal behaviors under an internal shorting process, thermal modeling of the internal shorting process for lithium-ion battery cell with cold-plate cooling is performed. The geometry and mesh for the modeling are shown in Figure 10. An aluminum cold plate is considered with mini-channels embedded inside for supplying cooling water. More physical properties and conjugate heat transfer modeling method used in the simulations can be found in reference [18].

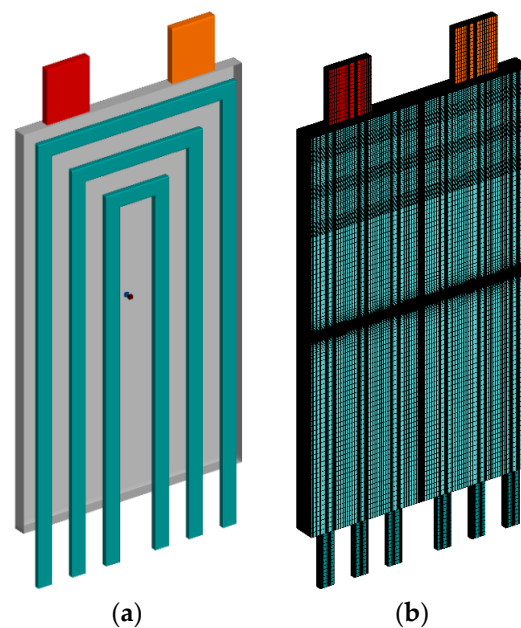


Figure 10. Schematic of (a) geometry; (b) mesh for internal shorting modeling of lithium-ion battery cooled by mini-channel cold plate.

It is seen in Figure 11 that the temperature evolutions are quite similar under different cooling conditions. Raising the convective heat-transfer coefficient from $17 \text{ W}/(\text{m}^2 \cdot \text{K})$ to $30 \text{ W}/(\text{m}^2 \cdot \text{K})$ helps to slightly reduce the maximum temperature on lithium-ion battery cell. Then, applying the mini-channel cold plate further brings down the maximum temperature in the cell. However, the difference in the maximum temperature in the cell is quite small, especially with respect to the change of mini-channel coolant velocity. The small effect of the mini-channel coolant velocity is firstly because the heat-transfer coefficient provided by the mini-channel is limited. In addition, the temperature rise of the coolant from the inlet to the outlet is not big, especially compared with the maximum cell temperature of above $300 \text{ }^\circ\text{C}$. Thus, unlike the situation under a fast discharging or external shorting condition where mini-channel flow rate has a large effect on lowering the cell temperature [17], the mini-channel flow rate does not succeed in reducing the cell temperature in the internal shorting process. Actually, the cooling solutions including enhancing the heat-transfer coefficient or adopting cold-plate cooling do not have large effects on alleviating the high temperature inside the lithium-ion battery cell. The conductive thermal resistance dominates the thermal behaviors of the internal shorting process, instead of the external cooling conditions.

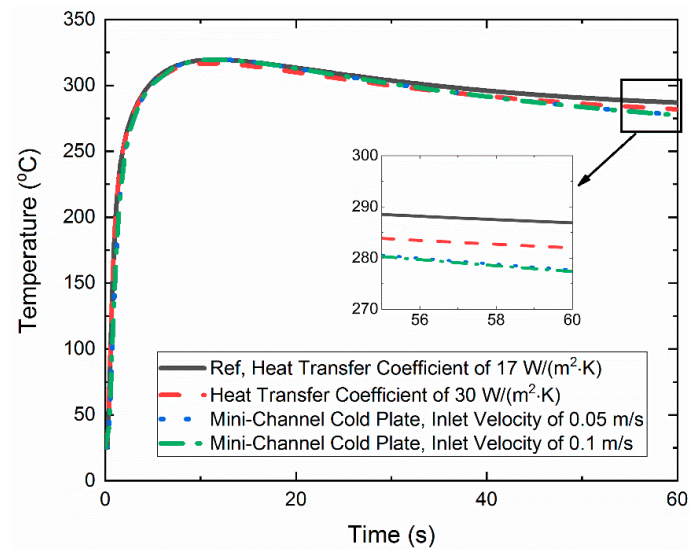


Figure 11. Modeling predicted maximum temperature on lithium-ion battery cell with different cooling schemes.

Figure 12 shows the temperature distribution evolutions for the lithium-ion battery cooled by a mini-channel cold plate undergoing the internal shorting process. The temperature contour is significantly governed by the internal shorting and it is hard to distinguish the coolant inlet to outlet direction temperature non-uniformity in Figure 12. This is because the internal shorting process creates a large temperature non-uniformity, which is much larger than the coolant inlet to outlet temperature non-uniformity. In comparison with Figure 6, the high temperature region above 100 °C in Figure 12 has a smaller area compared with the case of air cooling. The temperature above 100 °C will cause dangerous situations for triggering further lithium-ion battery thermal runaway. From this point of view, the mini-channel cold plate has advantage of better suppressing the area of high temperature region in the internal shorting process. The underlying reason is that the mini-channel cold plate employs an aluminum metal plate, which acts as a large heat spreader under the internal shorting condition. The aluminum metal plate helps to enhance the in-plane spreading of heat, thus helping to limit the high-temperature area.

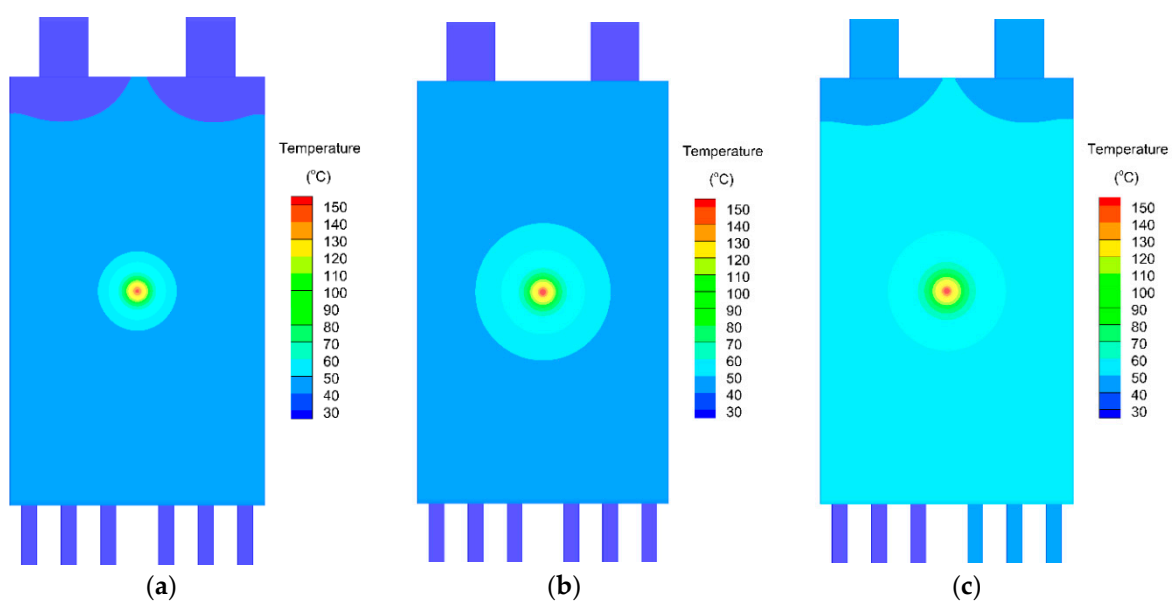


Figure 12. Temperature distributions of lithium-ion battery cooled by mini-channel cold plate with coolant velocity of 0.05 m/s at (a) 15 s; (b) 30 s; (c) 60 s.

4. Conclusions

With a multi-scale lithium-ion battery modeling framework, 3D thermal modeling of the internal shorting process in a realistic 20 Ah prismatic lithium-ion polymer battery is performed. In the subscale, the electrochemical effect is modeled with the ECM approach, while at the battery-cell scale, the electrical potentials and temperature fields are solved. The subscale and cell scale are connected with the volumetric current transfer rate and heat source terms. Simulations are run to investigate the effects of shorting resistance, through-plane thermal conductivity, and the mini-channel cold plate on the lithium-ion battery thermal responses in the internal shorting process. The thermal behaviors of the lithium-ion battery cell under an internal shorting process are found to be very sensitive to the quantity of the internal shorting resistance. A small shorting resistance will cause a large amount of heat generation and sudden rise of temperature near the internal short region. Then the heat conducts to the other regions in the battery cell. A great amount of heat released from the internal short and greatly localized temperature are the fundamental thermal features of the lithium-ion battery internal shorting process. It is found that the through-plane thermal conductivity significantly affects the maximum temperature evolution in the lithium-ion battery cell under internal shorting. As the through-plane thermal conductivity is very low, the through-plane heat conduction resistance is large and can dominate the heat resistance under internal shorting. On the other hand, the external cooling conditions have a relatively small effect on the maximum cell temperature evolutions, as pointed out in this study. This creates a situation quite different from the normal operation of a lithium-ion battery, where the cooling schemes are highly important and can be highly efficient in controlling cell temperature. The mini-channel cold-plate cooling also only has a small effect on suppressing the maximum temperature in a battery cell under internal shorting, regardless of its flow rate. However, the cold-plate cooling is found to be effective in suppressing the area of the overheated region by enhancing the in-plane heat spreading. Limiting the overheated region area is beneficial for reducing the risk of lithium-ion battery thermal runaway in the internal shorting process. The 3D thermal modeling approach developed in the present work is demonstrated to provide meaningful insights for the 3D temperature evolutions in a single battery cell with respect to the internal shorting process. Future work on 3D thermal simulations of an internal shorting process and thermal runaway process for the lithium-ion battery pack would be very valuable. This can provide further explanations of the thermal propagation mechanisms and lithium-ion battery pack thermal runaway mechanisms, which are not quite clear yet.

Author Contributions: Y.L. and Z.Z. undertook all the numerical simulations. Z.Z. derived all the equations. Y.L. undertook the validation. W.W. formed the conceptualization and supervised this work. All of the authors have provided substantial contributions to the manuscript preparation. All authors have read and agreed to the published version of the manuscript.

Funding: This research received no external funding.

Conflicts of Interest: The authors declare no conflict of interest.

References

1. Ji, Y.; Wang, C.Y. Li-ion cell operation at low temperatures. *J. Electrochem. Soc.* **2013**, *160*, A636–A649. [[CrossRef](#)]
2. Bandhauer, T.M.; Garimella, S.; Fuller, T.F. A critical review of thermal issues in lithium-ion batteries. *J. Electrochem. Soc.* **2011**, *158*, R1–R25. [[CrossRef](#)]
3. Wang, Q.; Jiang, B.; Yan, Y. A critical review of thermal management models and solutions of lithium-ion batteries for the development of pure electric vehicles. *Renew. Sustain. Energy Rev.* **2016**, *64*, 106–128. [[CrossRef](#)]
4. Karimi, G.; Li, X. Thermal management of lithium-ion batteries for electric vehicles. *Int. J. Energy Res.* **2013**, *37*, 13–24. [[CrossRef](#)]
5. Doyle, M.; Fuller, T.F.; Newman, J. Modeling of galvanostatic charge and discharge of the lithium/polymer/insertion cell. *J. Electrochem. Soc.* **1993**, *140*, 1526–1533. [[CrossRef](#)]

6. Fuller, T.F.; Doyle, M.; Newman, J. Simulation and optimization of the dual lithium ion insertion cell. *J. Electrochem. Soc.* **1994**, *141*, 1–10. [[CrossRef](#)]
7. Cai, L.; White, R.E. Mathematical modeling of a lithium ion battery with thermal effects in COMSOL Inc., multiphysics (MP) software. *J. Power Sources* **2011**, *196*, 5985–5989. [[CrossRef](#)]
8. Guo, M.; Kim, G.-H.; White, R.E. A three-dimensional multi-physics model for a li-ion battery. *J. Power Sources* **2013**, *240*, 80–94. [[CrossRef](#)]
9. Zhao, W.; Luo, G.; Wang, C.-Y. Effect of tab design on large-format Li-ion cell performance. *J. Power Sources* **2014**, *257*, 70–79. [[CrossRef](#)]
10. Li, Q.; Yang, C.; Santhanagopalan, S.; Smith, K.; Lamb, J.; Steele, L.A.; Torres-Castro, L. Numerical investigation of thermal runaway mitigation through a passive thermal management system. *J. Power Sources* **2019**, *429*, 80–88. [[CrossRef](#)]
11. Lee, K.-J.; Smith, K.; Pesaran, A.; Kim, G.-H. Three dimensional thermal-, electrical-, and electrochemical-coupled model for cylindrical wound large format lithium-ion batteries. *J. Power Sources* **2013**, *241*, 20–32. [[CrossRef](#)]
12. Allu, S.; Kalnaus, S.; Elwasif, W.; Simunovic, S.; Turner, J.A.; Pannala, S. A new open computational framework for highly-resolved coupled three-dimensional multiphysics simulations of Li-ion cells. *J. Power Sources* **2014**, *246*, 876–886. [[CrossRef](#)]
13. Xu, M.; Zhang, Z.; Wang, X.; Jia, L.; Yang, L. A pseudo three-dimensional electrochemical–thermal model of a prismatic LiFePO₄ battery during discharge process. *Energy* **2015**, *80*, 303–317. [[CrossRef](#)]
14. Basu, S.; Hariharan, K.S.; Kolake, S.M.; Song, T.; Sohn, D.K.; Yeo, T. Coupled electrochemical thermal modelling of a novel Li-ion battery pack thermal management system. *Appl. Energy* **2016**, *181*, 1–13. [[CrossRef](#)]
15. Zhao, J.; Rao, Z.; Li, Y. Thermal performance of mini-channel liquid cooled cylinder based battery thermal management for cylindrical lithium-ion power battery. *Energy Convers. Manag.* **2015**, *103*, 157–165. [[CrossRef](#)]
16. Rao, Z.; Wang, Q.; Huang, C. Investigation of the thermal performance of phase change material/mini-channel coupled battery thermal management system. *Appl. Energy* **2016**, *164*, 659–669. [[CrossRef](#)]
17. Qian, Z.; Li, Y.; Rao, Z. Thermal performance of lithium-ion battery thermal management system by using mini-channel cooling. *Energy Convers. Manag.* **2016**, *126*, 622–631. [[CrossRef](#)]
18. Li, Y.; Zhou, Z.; Wu, W.T. Three-dimensional thermal modeling of Li-ion battery cell and 50 V Li-ion battery pack cooled by mini-channel cold plate. *Appl. Therm. Eng.* **2019**, *147*, 829–840. [[CrossRef](#)]
19. Tobishima, S.I.; Yamaki, J.I. A consideration of lithium cell safety. *J. Power Sources* **1999**, *81*, 882–886. [[CrossRef](#)]
20. Feng, X.; Ouyang, M.; Liu, X.; Lu, L.; Xia, Y.; He, X. Thermal runaway mechanism of lithium ion battery for electric vehicles: A review. *Energy Storage Mater.* **2018**, *10*, 246–267. [[CrossRef](#)]
21. Feng, X.; Sun, J.; Ouyang, M.; Wang, F.; He, X.; Lu, L.; Peng, H. Characterization of penetration induced thermal runaway propagation process within a large format lithium ion battery module. *J. Power Sources* **2015**, *275*, 261–273. [[CrossRef](#)]
22. Feng, X.; He, X.; Ouyang, M.; Lu, L.; Wu, P.; Kulp, C.; Prasser, S. Thermal runaway propagation model for designing a safer battery pack with 25 Ah LiNi_xCo_yMn_zO₂ large format lithium ion battery. *Appl. Energy* **2015**, *154*, 74–91. [[CrossRef](#)]
23. Wang, Q.; Ping, P.; Zhao, X.; Chu, G.; Sun, J.; Chen, C. Thermal runaway caused fire and explosion of lithium ion battery. *J. Power Sources* **2012**, *208*, 210–224. [[CrossRef](#)]
24. Finegan, D.P.; Scheel, M.; Robinson, J.B.; Tjaden, B.; Hunt, I.; Mason, T.J.; Millichamp, J.; Di Michiel, M.; Offer, G.J.; Hinds, G.; et al. In-operando high-speed tomography of lithium-ion batteries during thermal runaway. *Nat. Commun.* **2015**, *6*, 6924. [[CrossRef](#)]
25. Hatchard, T.D.; MacNeil, D.D.; Basu, A.; Dahn, J.R. Thermal model of cylindrical and prismatic lithium-ion cells. *J. Electrochem. Soc.* **2001**, *148*, A755–A761. [[CrossRef](#)]
26. Spotnitz, R.; Franklin, J. Abuse behavior of high-power, lithium-ion cells. *J. Power Sources* **2003**, *113*, 81–100. [[CrossRef](#)]
27. Kim, G.H.; Pesaran, A.; Spotnitz, R. A three-dimensional thermal abuse model for lithium-ion cells. *J. Power Sources* **2007**, *170*, 476–489. [[CrossRef](#)]
28. Guo, G.; Long, B.; Cheng, B.; Zhou, S.; Xu, P.; Cao, B. Three-dimensional thermal finite element modeling of lithium-ion battery in thermal abuse application. *J. Power Sources* **2010**, *195*, 2393–2398. [[CrossRef](#)]

29. Lopez, C.F.; Jeevarajan, J.A.; Mukherjee, P.P. Characterization of lithium-ion battery thermal abuse behavior using experimental and computational analysis. *J. Electrochem. Soc.* **2015**, *162*, A2163–A2173. [[CrossRef](#)]
30. Xu, J.; Lan, C.; Qiao, Y.; Ma, Y. Prevent thermal runaway of lithium-ion batteries with minichannel cooling. *Appl. Therm. Eng.* **2017**, *110*, 883–890. [[CrossRef](#)]
31. Zhang, C.; Santhanagopalan, S.; Sprague, M.A.; Pesaran, A.A. Coupled mechanical-electrical-thermal modeling for short-circuit prediction in a lithium-ion cell under mechanical abuse. *J. Power Sources* **2015**, *290*, 102–113. [[CrossRef](#)]
32. Chen, M.; Sun, Q.; Li, Y.; Wu, K.; Liu, B.; Peng, P.; Wang, Q. A thermal runaway simulation on a lithium titanate battery and the battery module. *Energies* **2015**, *8*, 490–500. [[CrossRef](#)]
33. Coman, P.T.; Darcy, E.C.; Veje, C.T.; White, R.E. Numerical analysis of heat propagation in a battery pack using a novel technology for triggering thermal runaway. *Appl. Energy* **2017**, *203*, 189–200. [[CrossRef](#)]
34. Santhanagopalan, S.; Ramadass, P.; Zhang, J.Z. Analysis of internal short-circuit in a lithium ion cell. *J. Power Sources* **2009**, *194*, 550–557. [[CrossRef](#)]
35. Zavalis, T.G.; Behm, M.; Lindbergh, G. Investigation of short-circuit scenarios in a lithium-ion battery cell. *J. Electrochem. Soc.* **2012**, *159*, A848–A859. [[CrossRef](#)]
36. Zhao, W.; Luo, G.; Wang, C.Y. Modeling nail penetration process in large-format Li-ion cells. *J. Electrochem. Soc.* **2015**, *162*, A207–A217. [[CrossRef](#)]
37. Zhao, W.; Luo, G.; Wang, C.Y. Modeling internal shorting process in large-format Li-ion cells. *J. Electrochem. Soc.* **2015**, *162*, A1352–A1364. [[CrossRef](#)]
38. Kim, G.H.; Smith, K.; Lee, K.J.; Santhanagopalan, S.; Pesaran, A. Multi-domain modeling of lithium-ion batteries encompassing multi-physics in varied length scales. *J. Electrochem. Soc.* **2011**, *158*, A955–A969. [[CrossRef](#)]
39. Liaw, B.Y.; Nagasubramanian, G.; Jungst, R.G.; Doughty, D.H. Modeling of lithium ion cells—A simple equivalent-circuit model approach. *Solid State Ion.* **2004**, *175*, 835–839.
40. Hu, X.; Li, S.; Peng, H. A comparative study of equivalent circuit models for Li-ion batteries. *J. Power Sources* **2012**, *198*, 359–367. [[CrossRef](#)]
41. Taheri, P.; Bahrami, M. Temperature rise in prismatic polymer lithium-ion batteries: An analytic approach. *SAE Int. J. Passeng. Cars Electron. Electr. Syst.* **2012**, *5*, 164–176. [[CrossRef](#)]
42. Fink, C.; Kaltenecker, B. Electrothermal and electrochemical modeling of lithium-ion batteries: 3D simulation with experimental validation. *ECS Trans.* **2014**, *61*, 105–124. [[CrossRef](#)]
43. Dareini, A. *Prediction and Analysis of Model's Parameters of Li-ion Battery Cells*. Master of Science; Blekinge Institute of Technology: Blekinge, Sweden, 2016.
44. ANSYS, Inc. *Ansys Fluent 18.1 Advanced Add-on Module Guide Documentation*; ANSYS, Inc.: Canonsburg, PA, USA, 2017.



© 2020 by the authors. Licensee MDPI, Basel, Switzerland. This article is an open access article distributed under the terms and conditions of the Creative Commons Attribution (CC BY) license (<http://creativecommons.org/licenses/by/4.0/>).